U.S. DEPARTMENT OF ENERGY

PNNL-21446

Prepared for the U.S. Department of Energy
under Contract DE-AC05-76RL01830

Results of Laboratory Scale Fracture Tests on Rock and Cement Interfaces

W Um
HB Jung

June 2012

Pacific Northwest
NATIONAL LABORATORY

Proudly Operated by Battelle *Since 1965*

DISCLAIMER

This report was prepared as an account of work sponsored by an agency of the United States Government. Neither the United States Government nor any agency thereof, nor Battelle Memorial Institute, nor any of their employees, makes **any warranty, express or implied, or assumes any legal liability or responsibility for the accuracy, completeness, or usefulness of any information, apparatus, product, or process disclosed, or represents that its use would not infringe privately owned rights**. Reference herein to any specific commercial product, process, or service by trade name, trademark, manufacturer, or otherwise does not necessarily constitute or imply its endorsement, recommendation, or favoring by the United States Government or any agency thereof, or Battelle Memorial Institute. The views and opinions of authors expressed herein do not necessarily state or reflect those of the United States Government or any agency thereof.

PACIFIC NORTHWEST NATIONAL LABORATORY
operated by
BATTELLE
for the
UNITED STATES DEPARTMENT OF ENERGY
under Contract DE-AC05-76RL01830

Printed in the United States of America

Available to DOE and DOE contractors from the
Office of Scientific and Technical Information,
P.O. Box 62, Oak Ridge, TN 37831-0062;
ph: (865) 576-8401
fax: (865) 576-5728
email: reports@adonis.osti.gov

Available to the public from the National Technical Information Service
5301 Shawnee Rd., Alexandria, VA 22312
ph: (800) 553-NTIS (6847)
email: orders@ntis.gov <http://www.ntis.gov/about/form.aspx>
Online ordering: http://www.ntis.gov

This document was printed on recycled paper.
(8/2010)

PNNL-21446

Results of Laboratory Scale Fracture Tests on Rock and Cement Interfaces

W Um
HB Jung

June 2012

Prepared for the U.S. Department of Energy
under Contract DE-AC05-76RL01830

Pacific Northwest National Laboratory
Richland, Washington 99352

Contents

Figures

Tables

1.0 Methods and Material

1.1 Preparation of Cement Paste

The cement slurry was prepared by mixing Portland cement (Lafarge North America, type I-II) with water at a water-to-cement ratio of 0.38. A small quantity of cement slurry was thoroughly mixed by hand and cement samples were cast in the form of small-diameter cylinders by pouring the slurry into a plastic mold with or without a half-cylinder shaped basalt (Table 1.1). Cement samples were cured for 28 days under ambient conditions (20ºC and 1 atm).

Table 1.1. Summary of cement samples and compressive loading conditions. Bold numbers indicate the compressive load that caused major damage to cement samples.

Sample Number	Diameter	Length	Compressive Load 1	Compressive Load 2	Description
	mm		lbf		
1	13.7	50.2	**1613.8**		Pure cement
2	13.7	49.9	690.5	1098.5	Pure cement
3	13.7	49.5	528.3	**595.3**	Pure cement
4	13.7	50.0	349.9	**396.8**	Pure cement
5	13.7	50.1	301.3	497.2	Pure cement
7	24.8	17.8	299.4		Cement-basalt
8	24.8	20.7	**299.2**		Cement-basalt
9	14.4	15.9	599.6		Cement-basalt
10	13.7	14.2	**399.2**		Pure cement
11	13.7	13.0	499.4		Pure cement

1.2 Compressive Loading

A range of compressive loads was applied vertically to the specimen at 200 lbf/min to form internal fractures using servohydraulic test frames (MTS 10 Kip) with load cells (Lebow 10 Kip 3116). Compressive load testing was controlled by a system controller (Instron 8800) with Instron Bluehill 2 software, and stress-strain curves were collected (Figure 1.1). Before applying the compressive load, both ends of the cement columns were cut by a Buehler Isomet slow-speed saw with a diamond blade to achieve flat surfaces at both ends.

1.3 X-ray Microtomography

Cement samples were scanned using a high-resolution microfocus X-ray computed tomography (XCT) scanner (X-Tek/Metris XTH 320/225 kV) to visualize the formation and growth of internal fractures as a function of compressive loads. Scans were performed at 98-kV and 536-uA X-ray energy ranges with a 0.1-mm Cu filter for optimum image quality and contrast. The samples were rotated continuously during the scans with momentary stops to collect each projection (shuttling mode) to

minimize ring artifacts. A total of 3142 projections were collected over 360 degrees with 0.5 second exposure time and 1 frame per projection. Image voxel size varied between 10–25 microns depending on specimen dimensions. The images were reconstructed to get three-dimensional data sets using CT Pro 3D (Metris XT 2.2, Nikon Metrology, UK). Image stacks of two different orientations were created from the three-dimensional data using the visualization program VG Studio MAX 2.1 (Volume Graphics GmbH, Germany).

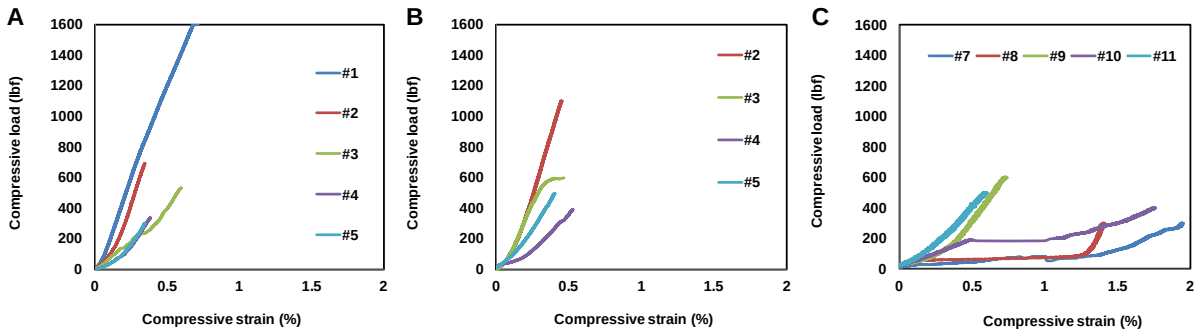

Figure 1.1. Stress-strain curves for pure cement columns (#1–5 and #10–11) and cement-basalt columns (#7–9) under compressive loads. Figures A and B are the results from the first and second compressive loading on sample #1–5, while Figure C is the result from the first compressive loading on sample #7–11.

2.0 Results

2.1 Fracture Growth in Pure Cement Column by Compressive Load

A total of 7 cement columns with a range of lengths (diameter: 13.7 mm; length: 13.0~50.2 mm) were subjected to compressive loads of approximately 300 to 1600 lbf. Although all cement columns were prepared and cured for 28 days under identical ambient conditions, the compressive strength of each specimen appears to be variable. For example, among cement columns with length-to-diameter ratios of 3.6, sample #1 showed major damage after a compressive load of 1614 lbf (no X-ray microfocus tomography [XMT] image was available because the sample completely collapsed), and sample #2 showed negligible structural damage after a compressive load of 1099 lbf (Figure 2.1). In contrast, samples #3 and #4 showed major damage after compressive loads of 595 lbf and 397 lbf, respectively (Figures 2.2 and 2.3). No visible fracture was formed in sample #5 under a compressive load of 301 lbf, but a thin vertical fracture began to form in the cement when the compressive load increased to 497 lbf (Figure 2.4).

Cement columns (samples #10 and #11) with length-to-diameter ratios of ~1:1 also show different compressive strengths although the columns were prepared and cured under identical conditions. Major fractures were formed in sample #10 after a compressive load of 399 lbf while there was no visible damage to sample #11 after a compressive load of 499 lbf (Figures 2.5 and 2.6). Variable compressive strengths of cement columns that were prepared and cured under the same conditions is attributable to heterogeneous micropore structure of the hydrated cement that develops during hydration of the anhydrous cement grains reacting with water. In addition, heterogeneous compressive strengths from different hydrated cement samples could also result from the nonuniform mixing of cement slurry.

Because of the heterogeneous nature of hydrated cement, this study focused on the fracture growth in each sample as a function of compressive loading, and did not attempt to compare the compressive strength between different cement samples. After a set of parallel fractures were formed near the top of samples #3 and #4 under compressive loads of 528 and 350 lbf, respectively, a slight addition of 50~70 lbf caused major damage to the cement structure, leading to the collapse of the cement columns (Figures 2.2 and 2.3).

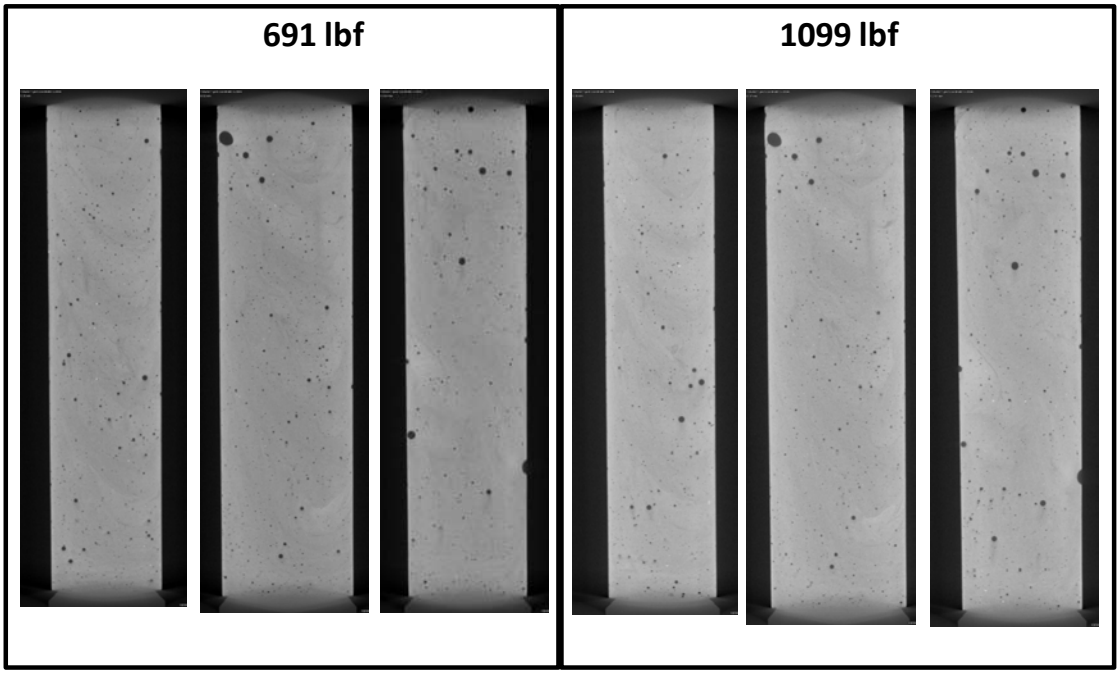

Figure 2.1. XMT images of a pure cement column (sample #2) after compressive loading at 691 lbf and 1099 lbf; XMT images before compressive loading are not available

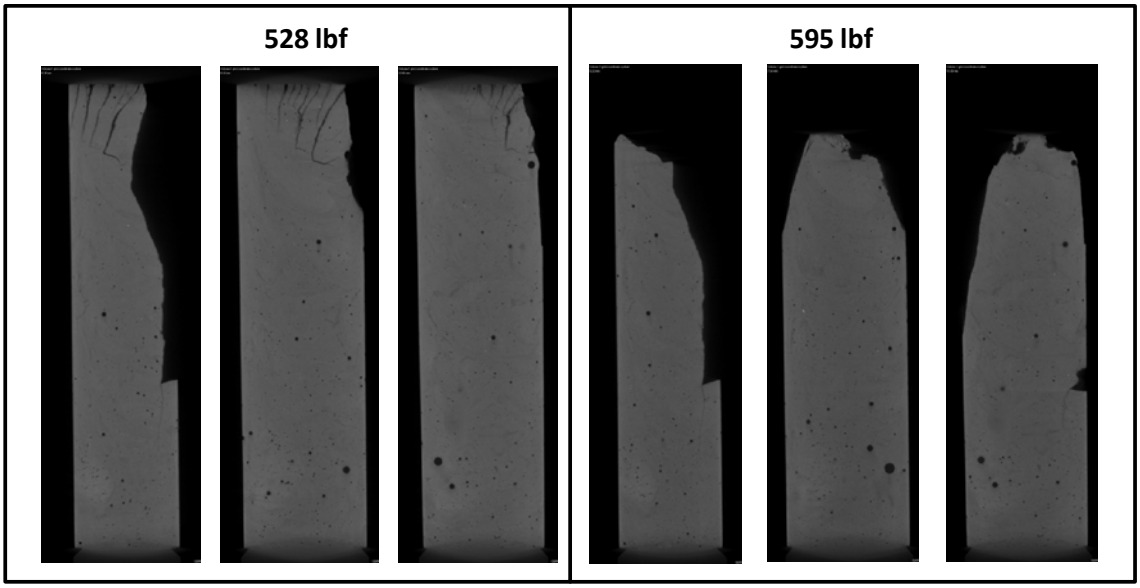

Figure 2.2. XMT images of a pure cement column (sample #3) after compressive loading at 528 lbf and 595 lbf; XMT images before compressive loading are not available

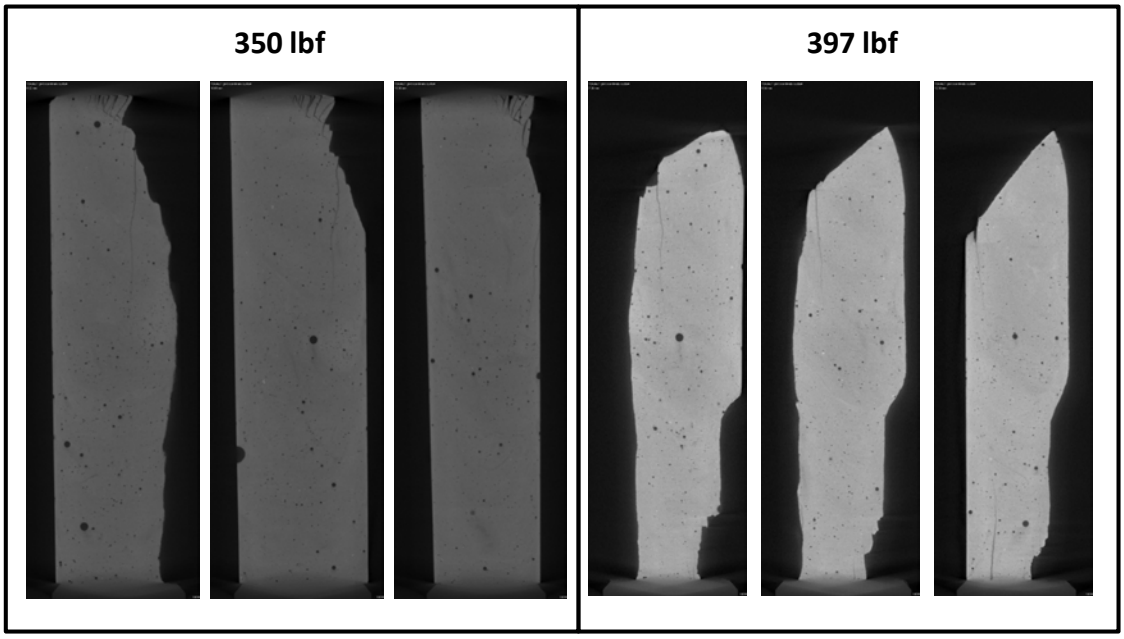

Figure 2.3. XMT images of a pure cement column (sample #4) after compressive loading at 350 lbf and 397 lbf; XMT images before compressive loading are not available. XMT scanning after compressive loading at 350 lbf and 397 lbf was not done at the same position due to severe structural damage of the specimen after compressive loading at 397 lbf.

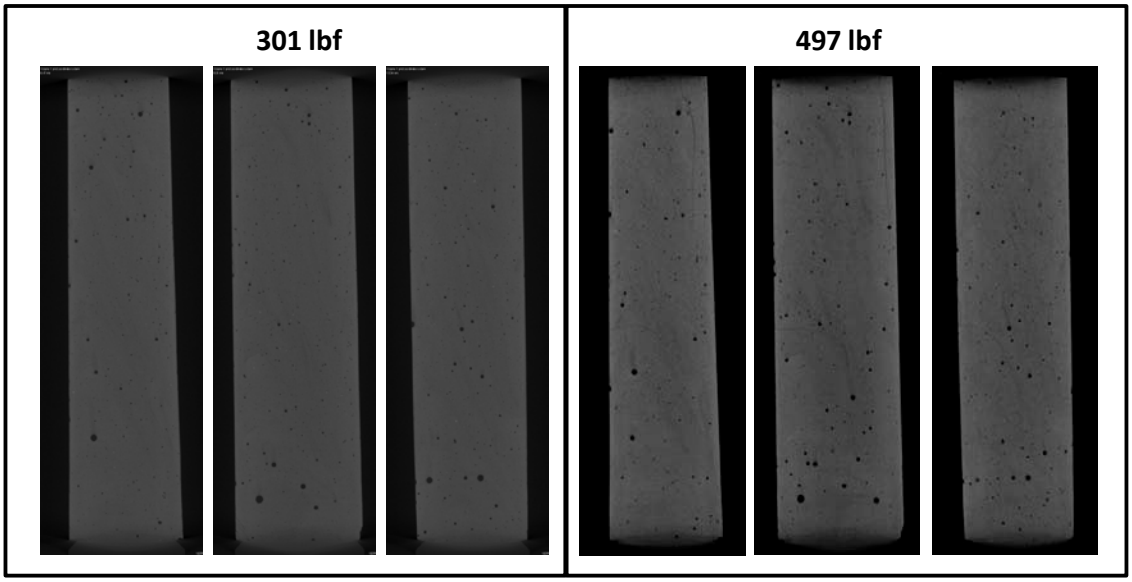

Figure 2.4. XMT images of a pure cement column (sample #5) after compressive loading at 301 lbf and 497 lbf; XMT images before compressive loading are not available

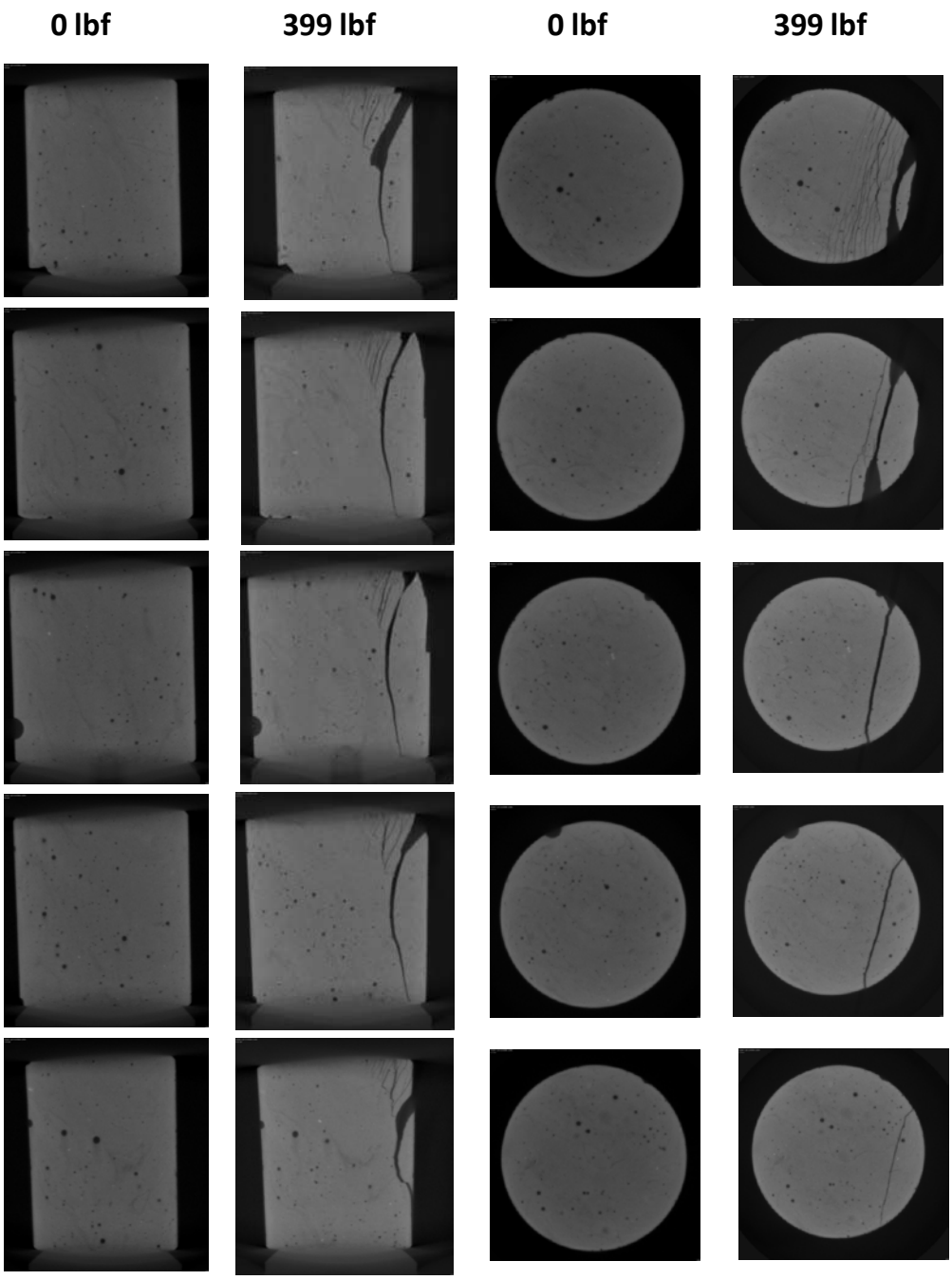

Figure 2.5. Vertical and horizontal XMT slices for sample #10 before and after compressive loading at 399 lbf

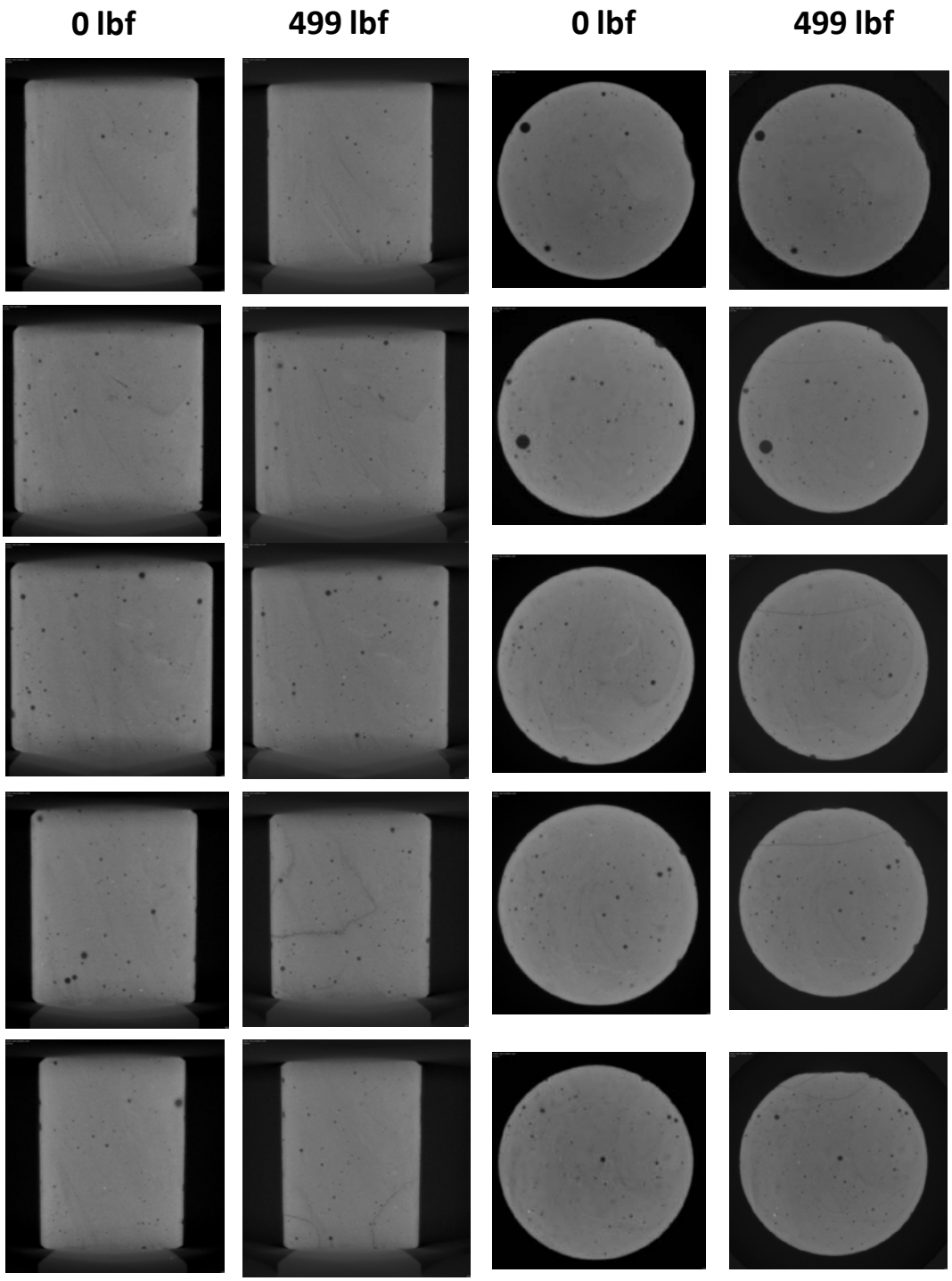

Figure 2.6. Vertical and horizontal XMT slices for sample #11 before and after compressive loading at 499 lbf

2.2 Fracture Growth in the Cement-Rock Interface Samples by Compressive Load

A total of three cement samples interfacing with basalt from the Wallula carbon sequestration pilot site were prepared under the same ambient conditions as pure cement columns. However, unlike pure cement columns, XMT images showed several initial fractures in the interface samples before compressive loading (Figures 2.7 and 2.8), possibly because of different elastic properties between cement and basalt. Fluid loss and shrinkage during cement hydration in the presence of basalt could also create fractures. For sample #9, which had a vertical interface between cement and basalt, the cement and basalt were separated during the cutting procedure prior to compressive loading due to weak bonding between hydrated cement and basalt fragments. Compressive loading was applied to this sample after combining the cement and basalt with transparent tape. XMT images of vertical and horizontal slices show the propagation of some initial fractures in vertical orientation near the outer boundary at 600 lbf, while it appears that most other initial fractures did not grow (Figure 2.7). Formation of new fractures and structural damage were observed from basalt rock near the interface with cement (Figure 2.7).

Sample #8 showed major initial fractures along the interface between cement and basalt almost from top to bottom, indicating a weak bond between cement and basalt, which is similar to sample #7. Although there was neither significant growth of fractures nor new formation of fractures under a compressive load of 299 lbf, damage of cement contacting basalt near the top of the cement column led to a vertical separation of the cement column into two parts (Figure 2.8). This result indicates that preferential flow paths for CO_2 or CO_2-rich water can be formed along the interface between cement and host rock in wellbore environments if the bond between the rock and cement is weak. Fractures tend to be formed along the interface between cement and rock during cement hydration, possibly due to different physical and chemical properties between cement and rock. If a major fracture is initially formed along the interface between cement and rock during cement hydration in wellbore environments, even a slight mechanical stress can cause significant damage to the wellbore and increase the risk of CO_2 leakage.

Sample #7 showed relatively good interface contact between cement and basalt, and the half-cylindrical basalt column was tilted at an angle of ~20 degrees during the curing process (Figure 2.9). Although there was no major structural damage to sample #7 under compressive loading of 299 lbf except separation of a small piece on the top, which was also observed in sample #8 (Figure 2.8), horizontal slices of XMT show a thin line of fracture was formed. Note initial fractures or newly formed fractures under compressive loads are extended from outer boundaries of the cement column to basalt inside the cement column (Figure 2.9). This indicates initial fractures or newly formed fractures in wellbore cement under compressive stress can be propagated to host rock, which can consequently decrease the integrity of wellbore and provide the pathway for CO_2 leakage.

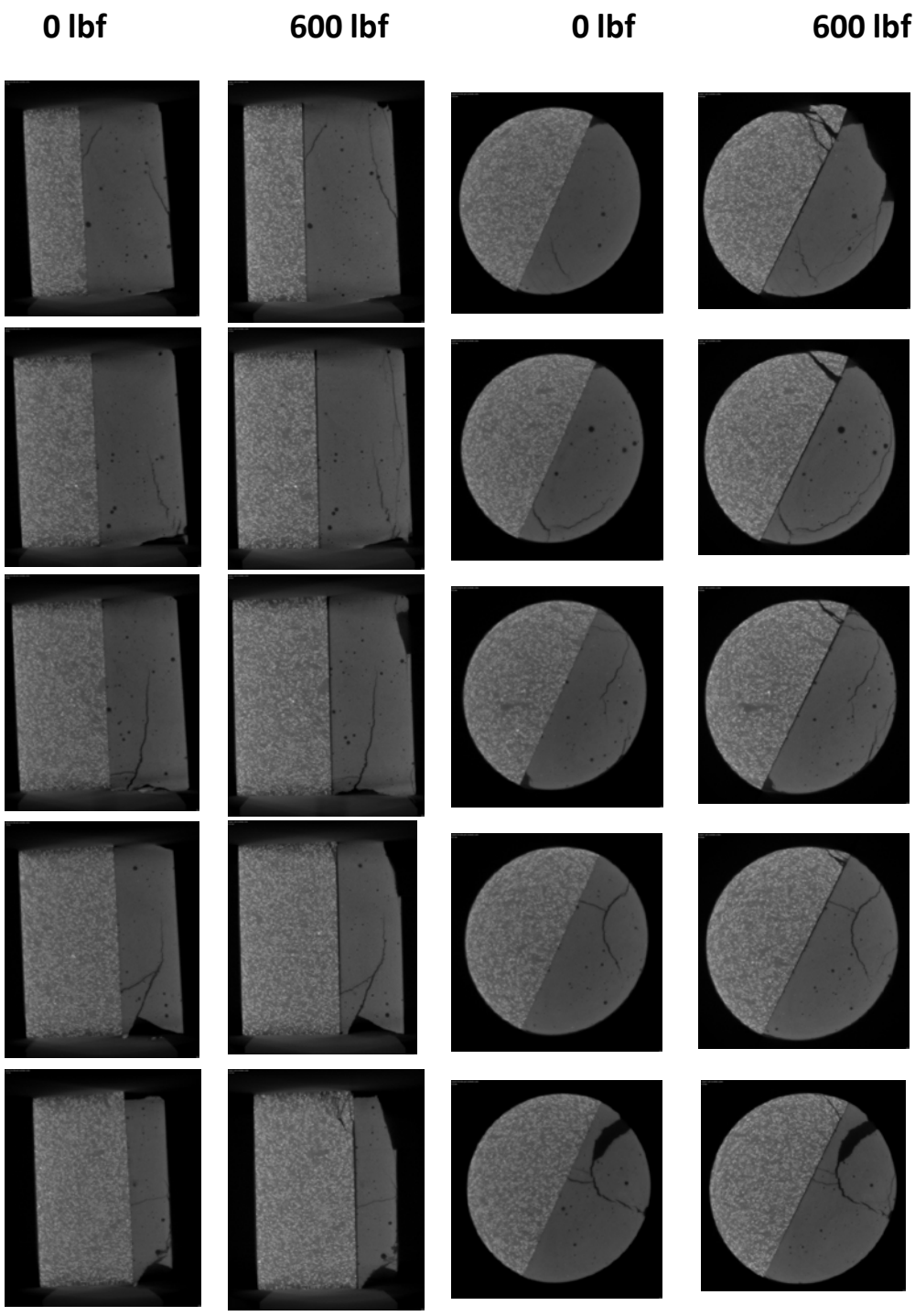

Figure 2.7. Vertical and horizontal XMT slices for sample #9 before and after compressive loading at 600 lbf. Lighter regions on the left side are basalt and darker regions on the right side are cement.

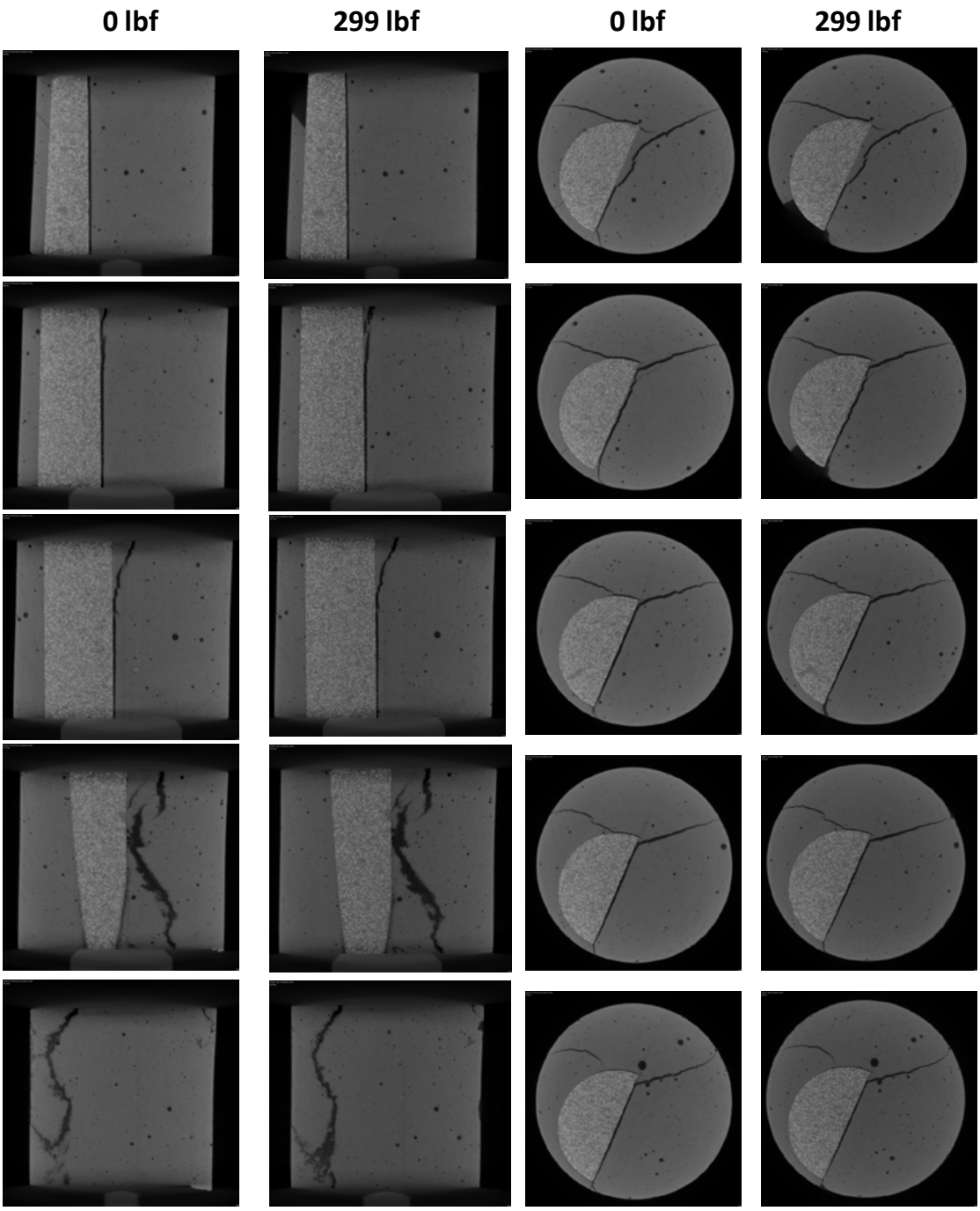

Figure 2.8. Vertical and horizontal XMT slices for sample #8 before and after compressive loading at 299 lbf

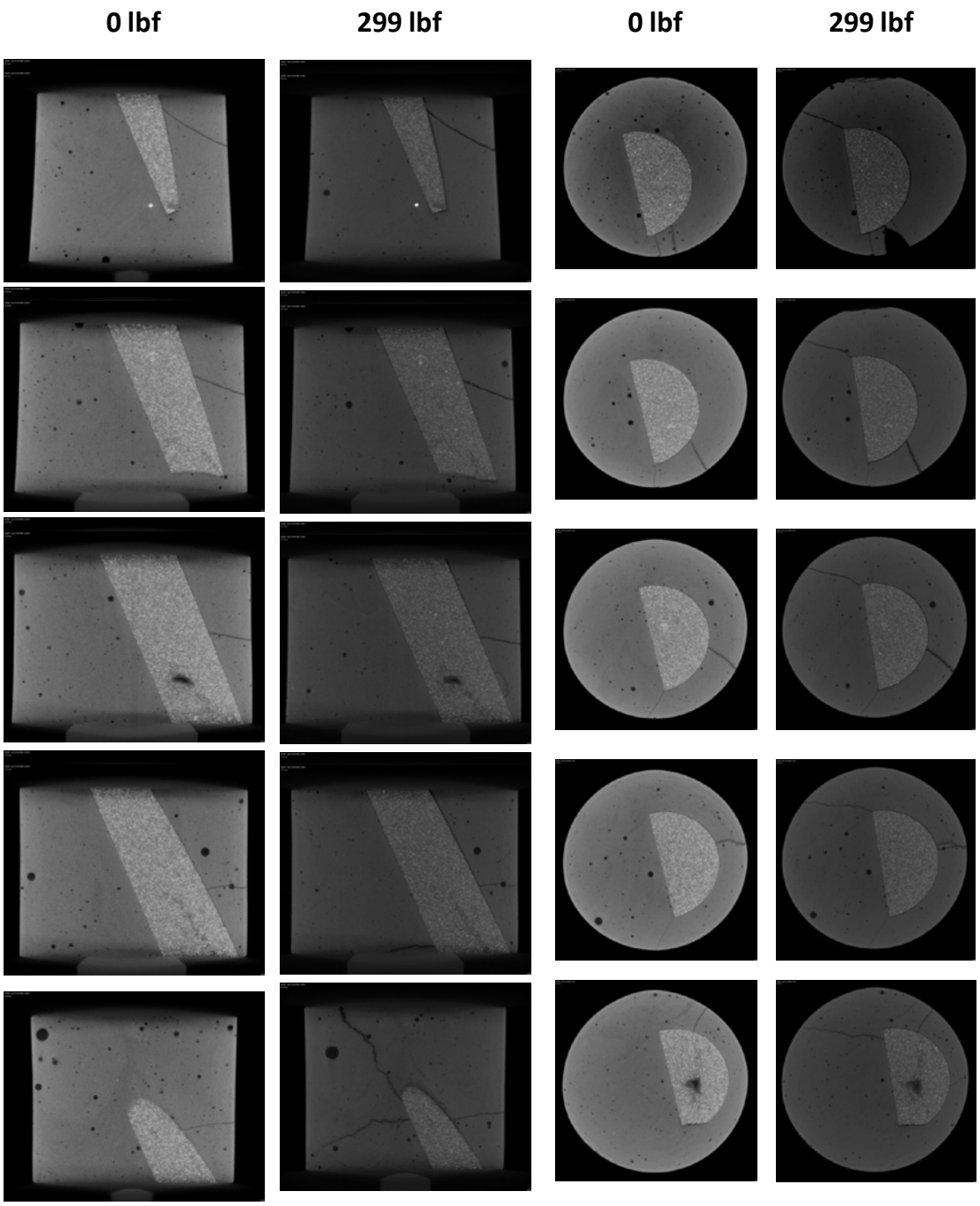

Figure 2.9. Vertical and horizontal XMT slices for sample #7 before and after compressive loading at 299 lbf

Distribution

No. of Copies

OFFSITE

3 Lawrence Berkeley National Laboratory
Earth Sciences Division
1 Cyclotron Road
Berkeley, CA 94720
- Curtis M. Oldenburg PDF
- Jim Houseworth PDF
- Preston D. Jordan PDF

2 Lawrence Livermore National Laboratory
7000 East Avenue
Livermore, CA 94550
- Susan A. Carroll PDF
- Stuart Walsh PDF

4 Los Alamos National Laboratory
P.O. Box 1663
Los Alamos, NM 87545
- Bill Carey PDF
- Amy B. Jordan PDF
- Rajesh Pawar PDF
- Philip H. Stauffer PDF

Brian Strazisar
National Energy Technology Laboratory
626 Cochrans Mill Road
P.O. Box 10940
Pittsburgh, PA 15236 PDF

No. of Copies

ONSITE

9 **Pacific Northwest National Laboratory**

- Christopher Brown PDF
- Pete McGrail PDF
- Kirk Cantrell PDF
- Chris Murray PDF
- Charlotte Sullivan PDF
- Wooyong Um PDF
- Hongbo Shao PDF
- Nik Qafoku PDF
- Hun Bok Jung PDF

Pacific Northwest
NATIONAL LABORATORY

Proudly Operated by Battelle *Since 1965*

U.S. DEPARTMENT OF
ENERGY

902 Battelle Boulevard
P.O. Box 999
Richland, WA 99352
1-888-375-PNNL (7665)
www.pnnl.gov